SCIENTIFIC REPORTS
nature research

OPEN

Effects of multiple injections on the efficacy and cytotoxicity of folate-targeted magnetite nanoparticles as theranostic agents for MRI detection and magnetic hyperthermia therapy of tumor cells

Meysam Soleymani[1,2], Solmaz Khalighfard[3,4], Saeed Khodayari[3,5], Hamid Khodayari[3,5], Mohammad Reza Kalhori[6], Mahmoud Reza Hadjighassem[2], Zhila Shaterabadi[7] & Ali Mohammad Alizadeh[2,3,8*]

Folate-targeted iron oxide nanoparticles (FA@Fe_3O_4 NPs) were prepared by a one-pot hydrothermal method and then used as cancer theranostic agents by combining magnetic resonance imaging (MRI) and magnetic hyperthermia therapy (MHT). Crystal structure, morphology, magnetic properties, surface functional group, and heating efficacy of the synthesized nanoparticles were characterized by XRD, TEM, VSM, FTIR, and hyperthermia analyses. The results indicated that the crystal structure, magnetic properties, and heating efficacy of the magnetite nanoparticles were improved by hydrothermal treatment. Toxicity of the prepared NPs was assessed *in vitro* and *in vivo* on the mammary cells and BALB/c mice, respectively. The results of the *in vitro* toxicity analysis showed that the FA@Fe_3O_4 NPs are relatively safe even at high concentrations of the NPs up to 1000 µg mL^{-1}. Also, the targetability of the FA@Fe_3O_4 NPs for the detection of folate over-expressed cancer cells was evaluated in an animal model of breast tumor using MRI analysis. It was observed that T_2-weighted magnetic resonance signal intensity was decreased with the three-time injection of the FA@Fe_3O_4 NPs with 24 h interval at a safe dose (50 mg kg^{-1}), indicating the accumulation and retention of the NPs within the tumor tissues. Moreover, the therapeutic efficacy of the MHT using the FA@Fe_3O_4 NPs was evaluated *in vivo* in breast tumor-bearing mice. Hyperthermia treatment was carried out under a safe alternating magnetic field permissible for magnetic hyperthermia treatment (f = 150 kHz, H = 12.5 mT). The therapeutic effects of the MHT were evaluated by monitoring the tumor volume during the treatment period. The results showed that the mice in the control group experienced an almost 3.5-fold increase in the tumor volume during 15 days, while, the mice in the MHT group had a mild increase in the tumor volume (1.8-fold) within the same period ($P < 0.05$). These outcomes give promise that FA@Fe_3O_4 NPs can be used as theranostic agents for the MRI and MHT applications.

[1]Department of Chemical Engineering, Faculty of Engineering, Arak University, Arak, 38156-88349, Iran. [2]Brain and Spinal Cord Injury research center, Neuroscience Institute, Tehran University of Medical Sciences, Tehran, Iran. [3]Cancer Research Center, Tehran University of Medical Sciences, Tehran, Iran. [4]Department of Biology, Islamic Azad University, Science and Research Branch, Tehran, Iran. [5]Electrophysiology Research Center, Neuroscience Institute, Tehran University of Medical Sciences, Tehran, Iran. [6]Medical Biology Research Center, Health Technology Institute, Kermanshah University of Medical Sciences, Kermanshah, Iran. [7]Department of Physics, Arak University, Arak, 38156-88349, Iran. [8]Breast Disease Research Center, Tehran University of Medical Sciences, Tehran, Iran. *email: aalizadeh@sina.tums.ac.ir

In recent years, magnetic nanoparticles (MNPs) have attracted considerable attention due to their potential application in the pharmaceutical and medicine fields such as magnetic hyperthermia therapy (MHT)[1,2], drug delivery systems[3–5], magnetic resonance imaging (MRI)[6,7], gene therapy[8], cell labeling[9], and immunoassay[10].

MHT has been investigated *in vivo* to treat several types of cancers, including breast, lung, brain, head and neck, prostate, pancreatic, and liver[11–18]. The principle of this method is based on the fact that cancerous cells are more sensitive to temperature rather than normal cells when the temperature is about 42–45 °C. In the MHT, magnetic nanoparticles must be introduced into the tumor tissue via systemic or direct injection and then subsequent exposure of the tumor tissue to high-frequency magnetic field results in heat generation by the MNPs via hysteresis losses, which can damage or kill cancer cells[19,20]. The heating efficiency of the MNPs under an alternating magnetic field is measured in terms of specific absorption rates (SAR). The value of this parameter is crucial for the hyperthermia application of MNPs and must be maximized because the higher SAR value leads to the smaller dose of the nanoparticles that must be injected into the body. The effects of particle size, shape, composition, and surface modification of the MNPs on the SAR value have been extensively studied by many researchers[21–23]. It has been found that MNPs in the single-domain ferromagnetic state with an open hysteresis loop can produce maximum heat under a safe alternating magnetic field[24]. Besides the appropriate size of MNPs for use in MHT, the effectiveness of this process depends upon the delivery of a sufficient dose of MNPs into the tumor tissue. The low dosage of MNPs that is accommodated into the tumor region cannot produce adequate heat in the tumor tissue, leading to the negligible or low efficacy of the treatment. Therefore, the accumulation of MNPs with appropriate size and concentration in the tumor tissue can affect the effectiveness of the MHT.

MNPs have also been used as MRI contrast agents for cancer diagnosis owing to their high r_2 relaxivity[6,7]. In a similar manner to the MHT, the major obstacles limiting the clinical application of the MNPs as a T_2-weighted contrast agent for MRI of tumors are the nonspecific accumulation and low concentration of the nanoparticles in the tumor tissue, causing no strong signal can be detected by the tumor tissue. One approach to enhance the accumulation of the nanoparticles in the tumor tissue is the incorporation of the tumor-specific targeting molecule on the surface of MNPs, resulting in specific uptake of the nanoparticles by cancer cells. Moreover, the tumor-targeted nanoparticles offer the advantages to decrease the side effects of the nanoparticles on normal cells. One of the favored candidates for active targeting of the MNPs is folic acid (FA), a kind of vitamin B complex, which has a high affinity to the folate receptor. Folate receptors are expressed at the relatively low levels in normal cells, but they are over-expressed in the surface of several cancer cells, including the ovary, breast, colon, lung, and brain[25]. Another approach that increases the number of nanoparticles in the tumor region is the successive injections of the targeted-nanoparticles at a safe dose, which can help the accumulation of the nanoparticles in the tumor tissue due to the enhanced permeability and retention (EPR) effects.

In the present work, dextran-coated Fe_3O_4 nanoparticles were synthesized using a one-pot hydrothermal method at 160 °C to produce stable and biocompatible magnetite nanoparticles with high heating efficacy for the MHT. Then, the folic acid was conjugated to the surface of the prepared nanoparticles via an esterification reaction. The prepared samples were thoroughly analyzed by different characterization analyses such as XRD, FTIR, TEM, and VSM. The *in vitro* and *in vivo* toxicity of the prepared nanoparticles were evaluated by the administration of different doses of the nanoparticles to the mammary cancer cells and BALB/c mice, and the cell viability and hematological/blood chemistry parameters were monitored. Moreover, the potential of the FA@Fe_3O_4 NPs to target the folate receptor cancer cells, as well as the effect of multiple injections on the accumulation of nanoparticles in the tumor tissue, was investigated by the MRI technique. Furthermore, the therapeutic efficacy of the MHT using the prepared nanoparticles was studied in breast tumor-bearing mice. The output of this study could be especially useful for improving the active-targeted MNPs as a single theranostic agent for combining MRI and MHT for the detection and treatment of cancer.

Results and Discussion

The Fe_3O_4 NPs can be synthesized by the different types of chemical methods[20,26,27]. Nanoparticles without any surface modification are not stable in the physiological media and readily aggregate. Therefore, the surface of the Fe_3O_4 NPs should be modified with a suitable coating that can enhance the stability of the nanoparticles and minimize their aggregation under the physiological conditions. In this study, we synthesized the dextran-coated Fe_3O_4 NP by *in situ* co-precipitation of the ferric and ferrous cations in the presence of the dextran molecules followed by the hydrothermal post-synthesis to increase the size, crystallinity, and purity of the synthesized sample. Finally, folic acid as a targeting moiety was conjugated to the hydroxyl groups of the dextran on the surface of Fe_3O_4 NPs by esterification reaction. The whole synthesis process is schematically shown in Fig. 1.

The crystal structure of the dextran-coated Fe_3O_4 NPs before (sample A) and after the hydrothermal treatment (sample B) was investigated by XRD analysis and the results are shown in Fig. 2a. In the XRD spectrum of sample A [Fig. 2a (i)], some impurity peaks related to the FeOOH phase (JCPDS 44-1416), the intermediate species created during the formation of the Fe_3O_4 NPs, were observed. On the other hand, in the XRD pattern of sample B [Fig. 2a (ii)], all reflection peaks can be indexed to a cubic structure of the Fe_3O_4 NPs (space group: Fd-3m) with characteristic peaks of (220), (311), (400), (422), (511), (440), (620), and (533) by referring to the JCPDS Card No. 75-0449. As can be seen, after the hydrothermal treatment, the intensity of the characteristic peaks of the Fe_3O_4 NPs was increased along with disappearing peaks belong to the FeOOH species.

It has been shown that the size, crystallinity, and the saturation magnetization (Ms) of magnetic nanoparticles can be increased by the hydrothermal method[28–30]. This technique is based on the Ostwald ripening mechanism in which the larger particles grow at the expense of the smaller ones. The average crystallite size of the product before and after hydrothermal treatment was estimated using the Debye-Scherrer's formula[31]:

$$D = 0.9\lambda/\beta cos\theta \quad (1)$$

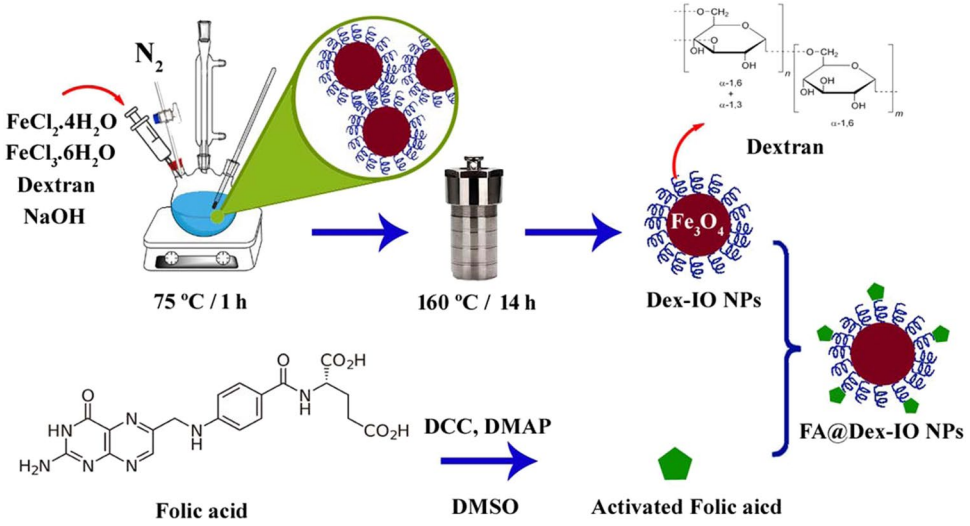

Figure 1. Synthesis process for the preparation of FA@Fe_3O_4 NPs.

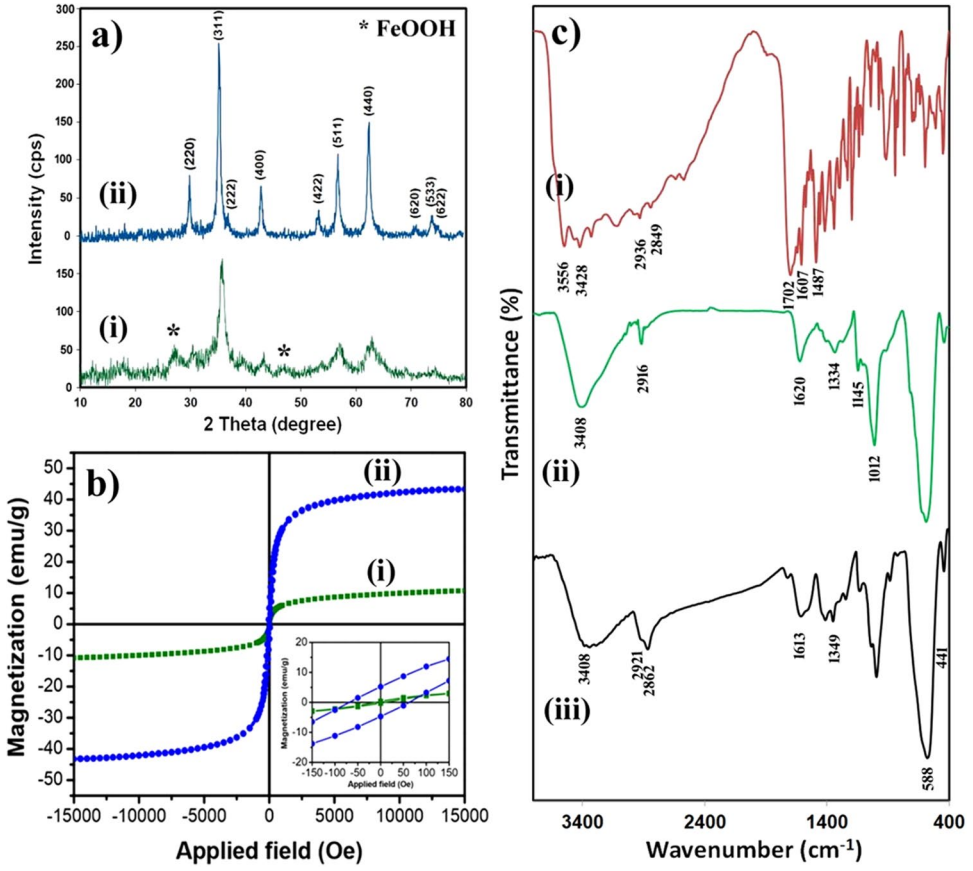

Figure 2. (**a**) XRD spectra of (i) sample A, and (ii) sample B, (**b**) Magnetization curves of (i) sample A, and (ii) sample B, the inset shows the magnified hysteresis loop of both samples, (**c**) FTIR spectra of (i) folic acid, (ii) dextran-coated Fe_3O_4 NPs, and (iii) FA@Fe_3O_4 NPs.

Where λ is the wavelength of Cu-Kα radiation (λ = 1.54178 Å), and θ and β represent the Bragg's angle and the full width at half maximum (FWHM) of the considered peak. The main diffraction peaks of each sample were employed for calculation. The average crystallite size of the Fe_3O_4 NPs before (sample A) and after (sample B) hydrothermal treatment was calculated to be about 8.6 and 21.1 nm, respectively. As can be seen, the crystallite size of the ferrite nanoparticles was significantly increased after hydrothermal treatment. Similar results were reported by other researchers[28–30,32].

	Sample A	Sample B
H_c (Oe)	11.0	65.0
M_r (emu/g)	0.3	9.0
M_s (emu/g)	10.4	43.0

Table 1. Magnetic parameters of the samples A and B.

The VSM analysis was performed on the prepared nanoparticles to evaluate the effects of the hydrothermal treatment on the magnetization behavior of samples A and B. The results of the VSM analysis have presented in Fig. 2b, and the main magnetic parameters have summarized in Table 1. The inset of Fig. 2b shows the magnified view of the central region of the hysteresis loops for both samples. As can be observed, after the hydrothermal treatment, the saturation magnetization and coercivity (Hc) of the nanoparticles were significantly increased from 10.4 to 43.0 emu g^{-1} and 11.0 to 65.0 Oe, respectively.

The increase of Ms can be related to the conversion of FeOOH (secondary phase observed in sample A, prepared before hydrothermal treatment) to Fe_3O_4 phase as well as the increase of particle size of Fe_3O_4 NPs during the hydrothermal treatment. In fact, by increasing the particle size of nanoparticles, the surface-to-volume ratio decreases which can result in a reduction of the surface effects such as spin disorder and dead layer on the surface, leading to an increase of the magnetization[33]. Increasing the Ms is frequently considered as a straightforward approach for improving the heat generated by the MNPs[34–36].

It has been shown that, when the size of the MNPs increases and they depart from the superparamagnetic regime, the coercivity (Hc) increases and reaches a maximum value at the single-domain ferromagnetic state and then decreases[30]. As can be observed in Table 1, the coercivity of the Fe_3O_4 nanoparticles increased along with the increasing of the particle size after hydrothermal treatment. The increase of the Ms and Hc in the MNPs is desirable for the theranostic (diagnostic and therapeutic) applications such as combining the MRI and magnetic hyperthermia therapy, in which MNPs with higher Hc and Ms produce higher signal intensity in the MRI applications and also MNPs with higher Ms, shape and magnetocrystalline anisotropy and enlarged hysteresis loop area have higher dissipation heat under alternating magnetic field with enough magnitude[33,37–39]. Based on the XRD and VSM results, sample B was chosen as the theranostic agent for the MRI and MHT experiments.

Folic acid was conjugated to the abundant hydroxyl groups of the dextran-coated on the surface of nanoparticles (sample B) using the esterification reaction. The FTIR spectroscopy was used to confirm the coating of the dextran as well as the further immobilizing of the folic acid on the surface of the Fe_3O_4 NPs.

The FTIR spectra of the pure folic acid, dextran-coated Fe_3O_4 NPs, and FA@Fe_3O_4 NPs are shown in Fig. 2c. In the FTIR spectrum of pure folic acid [Fig. 2c (i)], the absorption bands at 3556 and 3428 cm^{-1} are related to the stretching vibration of the hydroxyl groups (-OH) and N-H bonds, respectively. The absorption bands at 2936 and 2849 cm^{-1} are assigned to the asymmetric and symmetric vibrational modes of the $-CH_2$ groups. Also, the strong absorption peak that appeared at 1702 cm^{-1} is attributed to the stretching vibration of the carbonyl group (C=O) in the glutamic acid moiety of the folic acid, and the absorption peak at 1607 cm^{-1} is related to the bending vibrations of the –NH bond. Moreover, the band appeared at 1487 cm^{-1} is a characteristic absorption band of the phenyl ring[40].

In the FTIR spectra of the dextran-coated Fe_3O_4 NPs [Fig. 2c (ii)] and FA@Fe_3O_4 NPs [Fig. 2c (iii)], two absorption bands appeared in the range of 400–900 cm^{-1} arises from metal-oxygen bonds in the spinel structure of Fe_3O_4 nanoparticles[41]. The strong band in the range of 500–800 cm^{-1} could be related to the stretching vibration of the Fe-O bond in tetrahedral sites (ν_1), and the small band observed in the range of 400–500 cm^{-1} is attributed to the vibration mode related to the Fe-O bond in octahedral sites (ν_2)[41]. Also, the broad absorption peak at 3408 cm^{-1} is a distinctive stretching vibration of the hydroxyl groups presented in the dextran. In the FTIR spectrum of the dextran-coated Fe_3O_4 NPs, the absorption peaks at 2916 and 1334 cm^{-1} are due to the stretching and bending vibration of the $-CH_2-$ groups, respectively. The peak at 1620 cm^{-1} is attributed to the bending vibrations of the adsorbed water molecules on the surface of nanoparticles. Moreover, the peaks were exhibited at 1145, and 1012 cm^{-1} correspond to the stretching vibration of the alcoholic hydroxyl group (C-OH). Together these results confirm that the dextran was successfully coated on the surface of the Fe_3O_4 NPs.

The FTIR spectrum of the FA@Fe_3O_4 NPs presents all the characteristic absorption peaks of the FA and dextran-coated Fe_3O_4 NPs. The bands at 2921 and 2862 cm^{-1} are related to the stretching vibration of the $-CH_2-$ groups in the FA and dextran structures. After conjugation of folic acid to the dextran, a new absorption peak around 1702 cm^{-1} was added to the FTIR spectrum of the dextran-coated Fe_3O_4 NPs, which is related to the stretching vibration of carbonyl (C=O) bond in the ester group of FA, indicating the conjugation of the FA to the hydroxyl groups of dextran[42–44]. FTIR results proved that folic acid molecules have successfully immobilized on the surface of the dextran-coated Fe_3O_4 NPs.

The TEM image of the FA@Fe_3O_4 NPs and the corresponding particle size distribution measured by more than 300 particles from several pictures are shown in Fig. 3a. As can be observed, the FA@Fe_3O_4 NPs have an irregular shape with an average particle size of about 22 nm. The hydrodynamic diameter of the FA@Fe_3O_4 NPs was also measured by DLS analysis, and the result is shown in Fig. 3b. As can be seen, this sample has a relatively sharp peak around 68.1 nm with a size distribution in the range of 50 to110 nm and mostly in the range of 60 to 90 nm. As can be observed, the size measured by the DLS analysis is larger than that obtained by TEM analysis. This issue could be due to the tendency of particles to agglomerate in the solution, water hydration, and surface charge of the nanoparticles. The impacts of the particle size on the durability of the nanoparticles in the body were investigated by several authors[45–47]. The optimum particle size of the NPs for long blood circulation time was

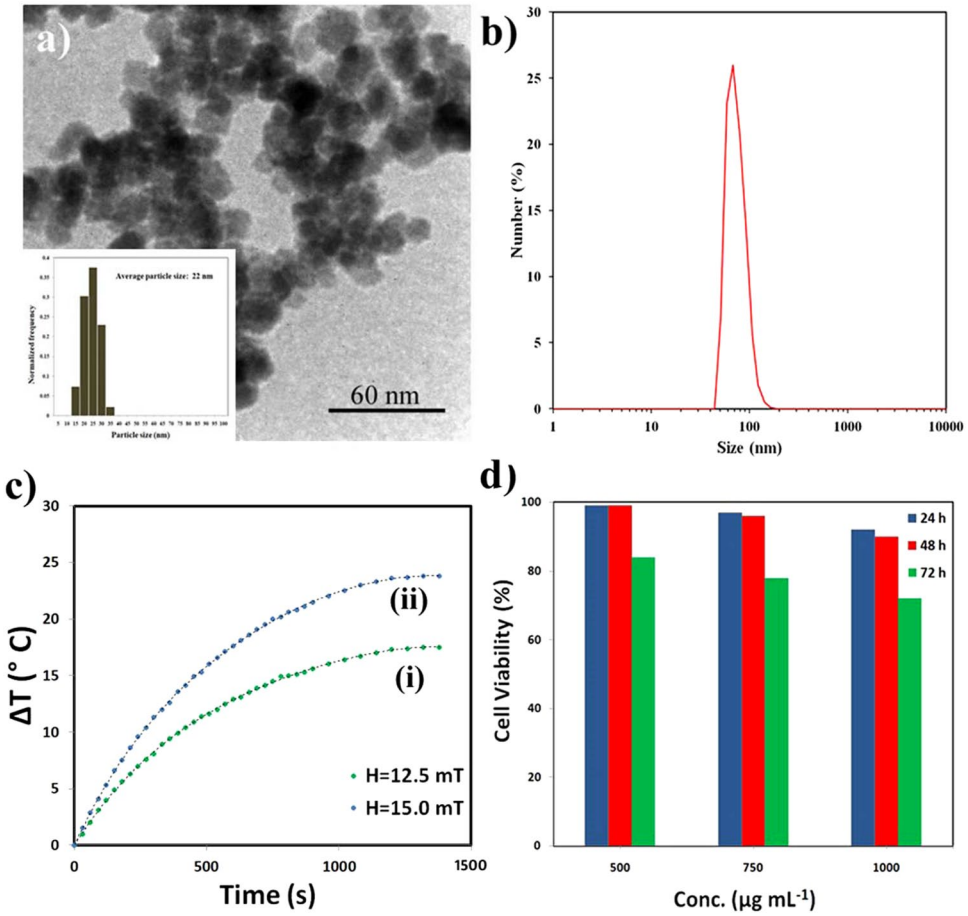

Figure 3. (**a**) TEM image and (**b**) particle size distribution of the FA@Fe_3O_4 NPs, (**c**) temperature rise vs. time curves of the magnetic suspension containing FA@Fe_3O_4 NPs (4 mg mL^{-1}), and (**d**) cell viability of MC4-L2 cells after exposing to the FA@Fe_3O_4 NPs at different concentrations and times.

found in the range of 10–100 nm[45–47]. Therefore, the prepared sample in the present study has suitable dimensions for biomedical applications.

The heat generation capability of the synthesized nanoparticles was investigated under two alternating magnetic fields. In this study, the safe magnetic fields with amplitudes of H = 12.5 and 15.0 mT at a fixed frequency (f = 150 kHz), which are permissible for hyperthermia therapy, were used[48,49].

After applying the magnetic field, the temperature rise of the magnetic suspension containing FA@Fe_3O_4 NPs (4 mg mL^{-1}) as a function of time was recorded, and the results are depicted in Fig. 3c. As can be seen, by increasing the magnetic field intensity, the higher temperature level was attained by the sample. It should be noted that the heating efficacy of the sample A (dextran-coated Fe_3O_4 NPs before hydrothermal treatment) was measured at the same magnetic fields, and a very low-temperature rise was observed during the experiments. This phenomenon can be related to the low magnetization and pure superparamagnetic behavior of sample A under the applied alternating magnetic field.

The SAR values calculated according to Eq. 2 for magnetic fields of H = 12.5 and 15.0 mT were 37.6 and 52.3 W g^{-1}, respectively. As can be seen, the SAR value improves by increasing the magnetic field intensity. It has been found the SAR values of magnetic NPs enhance with increasing the frequency (f) and the strength of the applied magnetic field (H)[50,51]. However, for clinical application of MHT, there are two rigid and less rigid criteria for the product of the intensity (H) and frequency (f) of the applied magnetic field which called the Atkinson–Brezovich limit ($H \times f = 4.85 \times 10^8$ $Am^{-1}s^{-1}$) and the Hergt's limit ($H \times f = 5 \times 10^9$ $Am^{-1}s^{-1}$), respectively[48,49]. More recently, Bellizzi and co-workers have performed a numerical study for determining the optimal frequency and magnetic field amplitude in MHT applied to the clinically relevant case of brain tumors[52]. They showed that the allowable values for $H \times f$ might be two to four times larger than the safety threshold of the Atkinson–Brezovich limit (4.85×10^8 $Am^{-1}s^{-1}$) which usually considered. The possibility of using higher $H \times f$ allows us to reduce the required dosage of MNPs for an effective MHT.

The SAR values of our sample and some distinguished studies, as well as commercial Fe_3O_4 nanoparticles (Feridex), are presented in Table 2. As can be observed, the SAR values reported for some magnetic nanoparticles are higher than the SAR values obtained in this study (Table 2). In most cases, it can be due to the use of larger magnetic fields so that the value of $H \times f$ is far from the Hergt's limit[48]. To better compare the heating efficiency of the FA@Fe_3O_4 NPs with other magnetic nanoparticles, the ILP value (normalized SAR) in each experiment was

Magnetic nanoparticles	Frequency(kHz)	Magnetic field (kAm^{-1})	$H \times f$ ($Am^{-1}s^{-1} \times 10^9$)	SAR (Wg^{-1})	ILP (nHm^2kg^{-1})	Reference
$FA@Fe_3O_4$	150	9.97	1.5	37.6	2.52	This study
$FA@Fe_3O_4$	150	11.96	1.8	52.3	2.44	This study
Fe_3O_4	300	15.0	4.1	168	2.48	[61]
$MgFe_2O_4$	700	5.0	3.5	11	0.9	[62]
$CoFe_2O_4$	370	20	7.4*	25	0.16	[63]
$Zn_{0.5}Ca_{0.5}Fe_2O_4$	354	10.2	3.6	14.8	0.4	[64]
$CaFe_2O_4$	354	10.2	3.6	24.5	0.66	[64]
$Gd_{0.02}Fe_{2.98}O_4$	370	50.0	18.5*	300	0.5	[65]
Ag/Fe_3O_4	313	40.1	12.5*	100	0.3	[66]
γ-Fe_2O_3	880	7.2	6.3*	210	4.6	[67]
γ-Fe_2O_3	500	15.7	7.8*	106	1.4	[68]
$CoFe_2O_4$@ $MnFe_2O_4$	500	37.3	18.7*	2280	3.28	[69]
$MnFe_2O_4$@ $CoFe_2O_4$	500	37.3	18.7*	3034	4.36	[69]
Feridex	—	—	—	—	0.15	[70]

Table 2. The magnetic field, SAR, and ILP values reported for several magnetic nanoparticles. *Larger than *Hergt's limit* (5×10^9 $Am^{-1}s^{-1}$).

calculated, and the results are presented in Table 2. As can be observed, $FA@Fe_3O_4$ NPs with ILP value about 2.5 nHm^2 kg^{-1} have an adequate intrinsic loss power among the other MNPs. Moreover, the ILP value of $FA@Fe_3O_4$ NPs is about 15 times higher than that of commercial Fe_3O_4 nanoparticles (Feridex) which have the FDA approval for biomedical applications, indicating the high potential application of the prepared sample for MHT.

It is crucial to evaluate the *in vitro* toxicity of the $FA@Fe_3O_4$ NPs before employing them to MRI and MHT applications. After treating MC4L2 cells with the $FA@Fe_3O_4$ NPs at the concentrations of 250, 500, and 1000 $\mu g\,mL^{-1}$ for 24, 48, and 72 h, the MTT assay was performed to investigate the cytotoxicity of the nanoparticles. As shown in Fig. 3d, passing the time and increasing the concentration of nanoparticles have a negative effect on the survival rate of the MC4L2 cells. Although the cell viability of the MC4L2 was decreased with increasing the concentration of the $FA@Fe_3O_4$ NPs in the medium, the concentration of 1000 $\mu g\,mL^{-1}$ of the sample is relatively safe, so that after 72 h more than 70% cells are still alive. It can be implied that the $FA@Fe_3O_4$ NPs have no cytotoxicity even at relatively high concentrations of the nanoparticles.

The primary outcomes of the *in vivo* toxicity related to the IP injection of the $FA@Fe_3O_4$ NPs at four administrative doses (10, 25, 50, and 100 $mg\,kg^{-1}$) on the hematologic and clinical parameters are depicted in Fig. 4, and the full results are presented in Table 3. As can be seen, within the chronic injection of the $FA@Fe_3O_4$ NPs, no significant changes in none of the mice assayed hematologic and biochemical factors in doses of 10, 25, and 50 $mg\,kg^{-1}$ were observed ($P > 0.05$). Only in mice treated with 100 $mg\,kg^{-1}$ $FA@Fe_3O_4$ NPs, a significant decrease in the ALP hepatic enzyme has assayed compared to the control group ($P < 0.05$). On the other hand, no inflammatory responses were observed in all chronic toxicity groups since total white blood cells were at a reasonable range. Besides, other clinical chemistry parameters, including hemoglobin, red blood cell counts, hematocrit, and platelet counts remained within the reasonable ranges even at a high dose of $FA@Fe_3O_4$ NPs (100 $mg\,kg^{-1}$). Based on the *in vitro* and *in vivo* toxicity results, a safe dose of $FA@Fe_3O_4$ NPs equal to 50 $mg\,kg^{-1}$ was chosen for the MRI and MHT experiments.

The potential application of the $FA@Fe_3O_4$ NPs to visualize the tumors with over-expressing folate receptors was evaluated in breast tumor-bearing mice. Figure 5 shows T_2-weighted magnetic resonance images of mice after receiving several constant doses (50 $mg\,kg^{-1}$) of $FA@Fe_3O_4$ NPs with 24 h interval. The tumor area of each mouse is shown by a white circle. The received dose in each injection was chosen based on the safe dosage, obtained in the *in vivo* toxicity experiments. The magnetic resonance image was taken after 24, 48, and 72 h of the first injection dose in each mouse. As shown in Fig. 5, the tumor tissue turned to dark in mouse with only one injection dose, suggesting the existence of the $FA@Fe_3O_4$ NPs in the tumor tissue.

Furthermore, the MRI signal intensity of the tumor in all mice is shown in Fig. 6. It can be observed that the MRI signal of the tumor region was significantly decreased by repeating the IP injection of the $FA@Fe_3O_4$ NPs, so that after three injections, the lowest intensity in the tumor area was obtained, indicating the more accumulation and retention of the $FA@Fe_3O_4$ NPs in the tumor tissue. These results revealed that the $FA@Fe_3O_4$ NPs have a high potential to target the breast tumors *in vivo* and can be used as a targeted MRI contrast agent in the diagnostic research.

To give more evidence of the *in vivo* targeting capability of the $FA@Fe_3O_4$ NPs for accumulation in the tumor site, the concentration of Fe in the tumor tissues of the "control group" and "nanoparticle group" (mice in the "nanoparticles group" received three doses of the $FA@Fe_3O_4$ NPs (50 $mg\,kg^{-1}$) with 24 h interval) was estimated using ICP-MS analysis. The quantitative analysis showed a significant difference ($P < 0.05$) of the Fe concentration in tumor tissue between control (0.7 mg_{Fe}/g_{Tumor}) and treated group (2.2 mg_{Fe}/g_{Tumor}). From the test tube experiments and *in vitro* cell hyperthermia analyses, it has been found that the minimum concentration of the iron required in the tumor tissue to produce adequate heat in the magnetic hyperthermia process must be in the range of 0.1–0.4 wt %[53–55]. According to the ICP-MS analysis results, after a three-time systemic injection of the

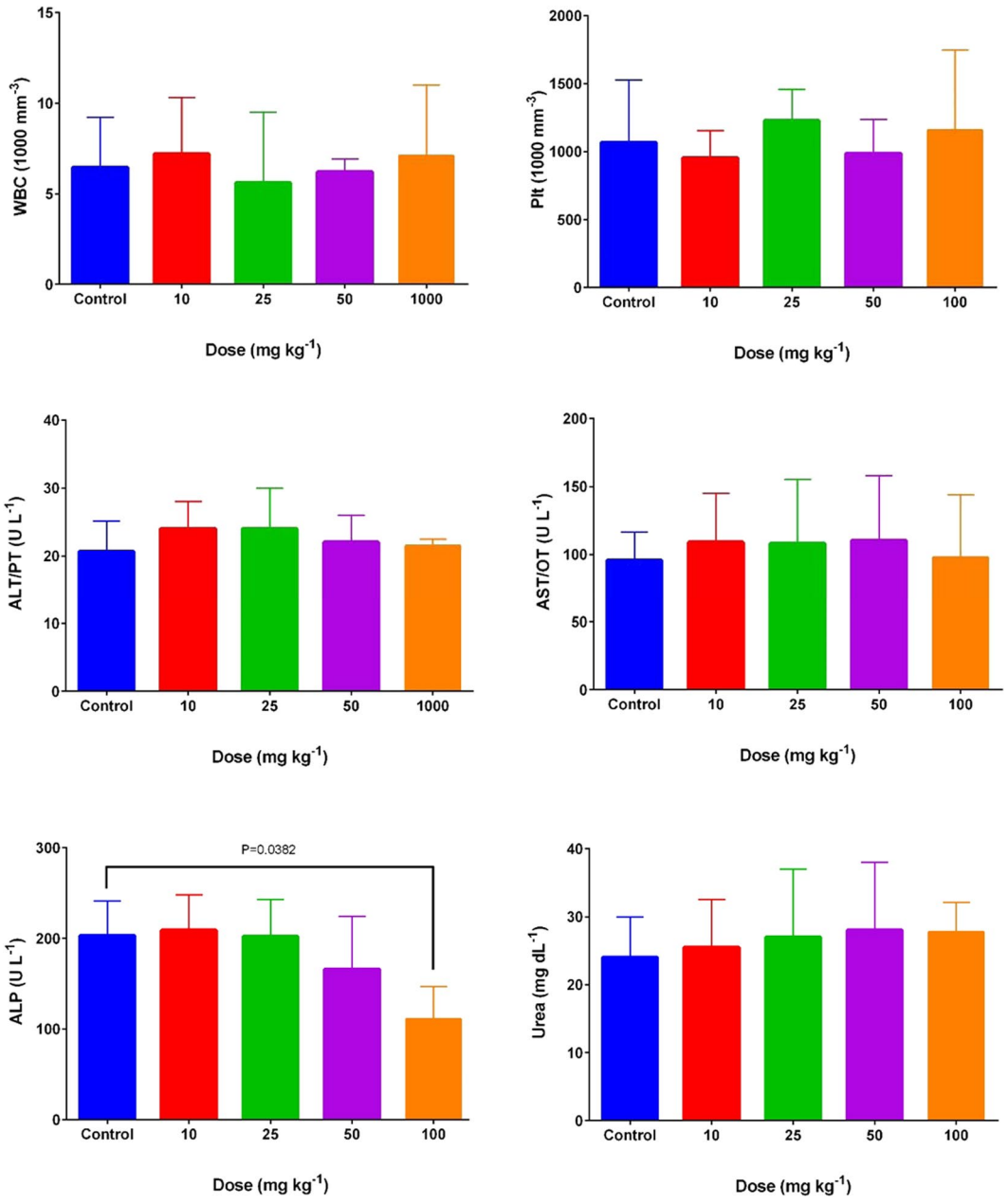

Figure 4. Chronic toxicity effects of FA@Fe_3O_4 NPs on the major hematological and blood biochemical parameters.

FA@Fe_3O_4 NPs into the body, a sufficient concentration of Fe (0.15 wt %, calculated based on the net Fe concentration accumulated in the tumor tissue) was prepared in the tumor tissue for the MHT.

The therapeutic activity of the FA@Fe_3O_4 NPs was evaluated in an animal model of breast cancer. Figure 7a,b show representative images of the magnetic hyperthermia unit and a mouse lying within the designed coil. During hyperthermia experiments, neither mortality nor any significant alteration in behavior was observed in all groups during the 15 days of treatment. The tumor growth rates of all groups are depicted in Fig. 7c, A significant difference in the tumor growth between the treated mice in the MHT group and the untreated mice in the control group can be observed. In the control group (mice did not receive magnetic hyperthermia treatment) and "MF group" (mice only exposed to the alternating magnetic field several times), the tumors grew progressively. Notably, the untreated mice in the control group experienced an almost 3.5-fold increase in the tumor volume over 15 days, whereas the mice in the MHT group had a moderate increase in the tumor volume (1.8-fold) within the same period. Moreover, the tumor growth rate of the "NPs group" and "MF group" was higher than the MHT group, indicating none of the FA@Fe_3O_4 NPs and magnetic field solely cannot suppress the tumor growth. These results showed the effectiveness of the MHT using the FA@Fe_3O_4 NPs for the treatment of the breast tumor.

Parameters	Control	10 (mg kg^{-1})	25 (mg kg^{-1})	50 (mg kg^{-1})	100 (mg kg^{-1})
WBC (1000/mm^3)	6.5 ± 2.7	7.2 ± 3.1	5.6 ± 3.9	6.2 ± 0.7	7.1 ± 3.9
% Lymph	63 ± 14	60 ± 16	70.5 ± 9.1	67 ± 10.4	63.3 ± 22
RBC (Millin/mm^3)	7.1 ± 1.4	6.9 ± 1	7.2 ± 1	6.7 ± 1.5	7.1 ± 1.6
Hgb (g/dL)	11.6 ± 1.9	11.1 ± 1	11.5 ± 1	10.2 ± 2.2	10.9 ± 2.1
HCT (%)	35.6 ± 5.2	33 ± 2.8	36.6 ± 3.2	31.9 ± 7.4	33.8 ± 8.3
MCV (FL)	49.8 ± 5.9	50.5 ± 5.6	51.2 ± 5.8	50 ± 4.7	49.1 ± 2.1
MCH (pg)	15.6 ± 2.5	15.9 ± 1.9	16.1 ± 2.3	15.9 ± 2.6	15.5 ± 2.9
MCHC (mol/L)	30.4 ± 1.7	31.6 ± 0.6	31.4 ± 0.9	31.8 ± 3	31.3 ± 2.3
PLT (1000/mm^3)	1066 ± 462	953 ± 199	1226 ± 232	986 ± 252	1155 ± 591
BUN (mg/dL)	24 ± 6	25.5 ± 7	27 ± 10	28 ± 10	29.6 ± 4
ALP (U/L)	203 ± 38	209 ± 39	202 ± 41	166 ± 58	111 ± 36*
AST (U/L)	95.5 ± 21	109 ± 36	108 ± 47	110 ± 48	98 ± 46
ALT (U/L)	21 ± 5	24 ± 4	20 ± 10	22 ± 4	21.5 ± 1
GLU (mg/dL)	74 ± 10	65 ± 41	84.5 ± 18	85 ± 14	67 ± 19
Ca (mM/L)	3.5 ± 0.9	3.7 ± 0.3	3.7 ± 0.5	3.8 ± 0.9	4.2 ± 1
Mg (mM/L)	0.95 ± 0.1	1.2 ± 0.2	1.1 ± 0.3	1.2 ± 0.6	1.1 ± 0.5
D.Bil (mg/dL)	0.04 ± 0.03	0.06 ± 0.02	0.07 ± 0.04	0.04 ± 0.02	0.06 ± 0.02
TP (mg/dL)	1.4 ± 0.1	1.4 ± 0.2	1.3 ± 0.1	1.1 ± 0.3	1.5 ± 0.04

Table 3. Hematological and blood chemical parameters for mice after different chronic doses of FA@Fe_3O_4 NPs. Values are means ± SD, and (*) indicates $P < 0.05$ compared to the control group. RBC = red blood cell, HCT = hematocrit, Hbg = hemoglobin, WBC = white blood cells, Plt = platelets, BUN = blood urea nitrogen, Cr = creatinine, Glu = glucose, AST = aspartate transaminase, ALT = alanine transaminase, ALP = alkaline phosphatase, Alb = albumin, T.P = total protein, B.T = Bilirubin Total, D.Bil = Direct Bilirubin. MCV = mean corpuscular volume, MCH = mean corpuscular hemoglobin, MCHC = mean corpuscular hemoglobin concentration, Ca = calcium, and Mg = magnesium.

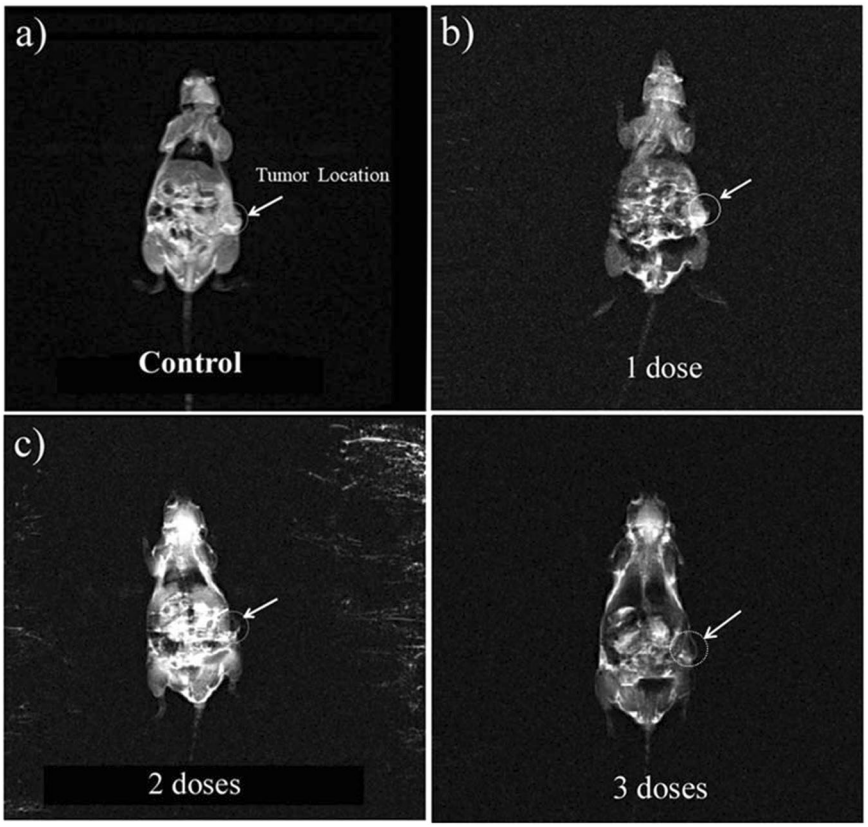

Figure 5. Magnetic resonance images of the mouse with a breast tumor, (**a**) mouse without injection dose (control), (**b**) mouse with one injection dose, (**c**) two injection doses, and d) three injection doses.

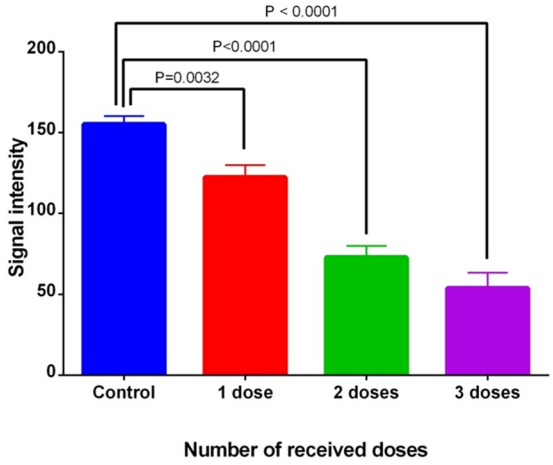

Figure 6. MRI signal intensity of the tumor tissue in the breast tumor-bearing mice with several receiving doses.

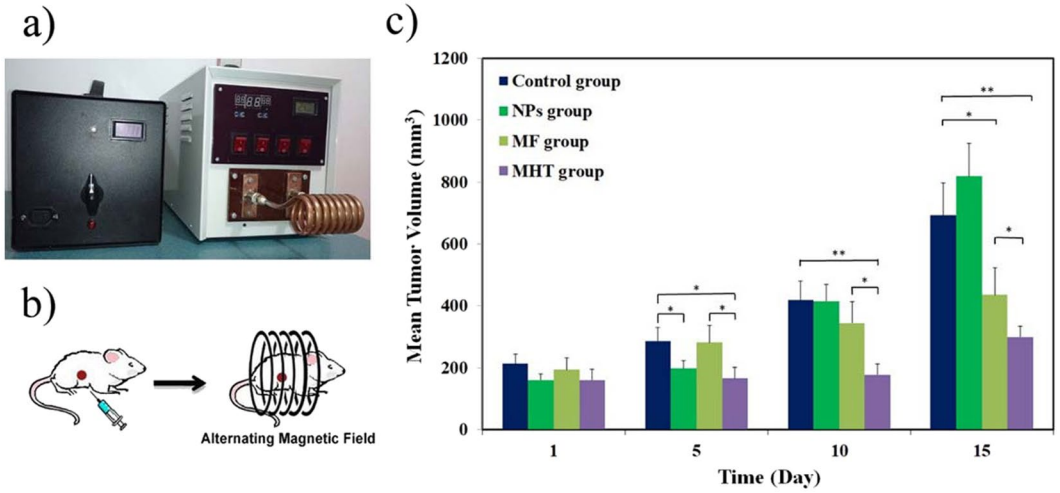

Figure 7. (**a**) magnetic hyperthermia unit used for *in vivo* MHT experiments, (**b**) Schematic of *in vivo* magnetic hyperthermia therapy on a mouse, and (**c**) The mean tumor volume vs days after onset of the treatment for all groups, (*) indicates $P < 0.05$, (**) indicates $P < 0.005$.

Conclusions

In this study, we have successfully prepared the theranostic FA@Fe_3O_4 NPs as negative contrast agents for MRI as well as nanoheaters for magnetic hyperthermia treatment. The results of the MTT analysis indicated that the FA@Fe_3O_4 NPs were relatively safe even at high concentrations of the nanoparticles up to 1000 μg mL^{-1}, satisfying one of the main requirements for biomedical applications. *In vivo* toxicity assessments revealed that the chronic toxicity of the FA@Fe_3O_4 NPs has appeared at the IP injection dose of 100 mg kg^{-1}. Likewise, other clinical chemistry parameters, including hemoglobin, red blood cell counts, hematocrit, and platelet counts remained within the normal ranges even at this dose. The *in vivo* MRI experiments showed a significant decrease in the T_2-weighted MR signal intensity of breast tumors by repeating the injection doses, indicating the accumulation and retention of the FA@Fe_3O_4 NPs in the tumor tissue. Moreover, hyperthermia treatment on an animal model of breast tumor using the FA@Fe_3O_4 NPs showed tumor progression could be reduced by this treatment.

Material and Methods

Materials. All used chemicals in this study were in the analytical grade, and they used without any further purification. Iron (III) chloride hexahydrate ($FeCl_3.6H_2O$), iron (II) chloride tetrahydrate ($FeCl_2.4H_2O$), sodium hydroxide (NaOH), dextran (Mw ≈ 10,000), folic acid (FA), *N, N*'-dicyclohexylcarbodiimide (DCC), anhydrous dimethyl sulfoxide (DMSO), 4-dimethylamino pyridine (DMAP), and MTT (3-(4,5-dimethylthiazole-2-yl)-2,5-diphenyltetrazolium bromide) powder were purchased from the Sigma-Aldrich Company. The MC4L2 cells were purchased from the Iranian Biological Resource Center (Tehran, Iran). Dulbecco's Modified Eagle Medium (DMEM) cell culture and FBS were purchased from Scotland (Gibco, Scotland).

The study design. The experimental studies done in this research can be categorized in four parts, including I: the preparation and characterization of the FA@Fe_3O_4 NPs, II: the *in vitro* and *in vivo* cytotoxicity evaluation of the FA@Fe_3O_4 NPs, III: the efficiency of the FA@Fe_3O_4 NPs for accumulation in the tumor tissues by the MRI analysis, and IV: the efficacy of the MHT by using the FA@Fe_3O_4 NPs for treatment of breast tumors.

Synthesis of dextran-coated Fe_3O_4 nanoparticles. The dextran-coated Fe_3O_4 nanoparticles were synthesized by *in situ* co-precipitation of the ferrous and ferric salts in the dextran solution[20]. Briefly, the $FeCl_2{\cdot}4H_2O$ (1.0 mmol) and $FeCl_3{\cdot}6H_2O$ (2.0 mmol) were mixed in a dextran solution and then heated to 80 °C. After purging the solution with nitrogen for one hour, NaOH solution (1.0 M) was subsequently added to the mixture. Formation of the Fe_3O_4 NPs was indicated by the color change of the solution from the light brown to black (obtained product at this stage was named as sample A). The black suspension was then undergone to the hydrothermal treatment by transferring it to the sealed autoclave and aging at 160 °C for 14 h. The obtained product after the hydrothermal treatment named sample B.

Synthesis of FA@Fe_3O_4 NPs. The conjugation of folic acid to the surface of dextran-coated Fe_3O_4 nanoparticles was performed by the esterification reaction between the carboxyl group of the folic acid and the hydroxyl group of the dextran[56]. Briefly, DCC (0.01 g), DMAP (0.005 g), and folic acid (0.02 g) were dissolved in the anhydrous DMSO and stirred under the N_2 atmosphere at room temperature overnight. Then, an aqueous solution of the dextran-coated nanoparticles (5 mg mL^{-1}) was added to the reaction mixture and stirred for 24 h at 80 °C under the N_2 atmosphere in the darkness. The prepared sample was washed with the ethanol and water three times and finally suspended in the distilled water (5 mg mL^{-1}) for further use.

Characterization of FA@Fe_3O_4 NPs. Crystallinity and phase purity of the prepared samples were investigated by the powder X-ray diffraction (XRD, Philips, X-pert) with the Cu-K α radiation and a Ni filter ($\lambda = 0.15418$ nm). Fourier Transform Infrared (FTIR) spectroscopy analysis was carried out on a Bruker Vertex 70 spectrometer in the range of 4000-400 cm^{-1}. The morphology and particle size of the samples were observed by a Transmission Electron Microscopy (TEM) with an acceleration voltage of 120 kV. The magnetic properties of the samples were measured by a vibrating sample magnetometer (VSM, Meghnatis Kavir Kashan Co., Iran) instrument at room temperature. The hydrodynamic size distribution of the prepared sample was measured by dynamic light scattering (DLS, Malvern zeta sizer-ZEN3600).

***In vitro* toxicity of FA@Fe_3O_4 NPs.** Through the Methyl ThiazolTetrazolium Bromide (MTT) assay, the cytotoxicity of the FA@Dex-IO NPs was evaluated on MC4-L2 cells. First, approximately 1×10^4 cells per well were seeded in a 96-well plate. The cells were cultured in the DMEM medium neutralized with 10% FBS and incubated at 37 °C for 24 h in a humidified 5% CO_2 atmosphere. Then, under treatment with various concentrations of the FA@Fe_3O_4 NPs (250, 500, and 1000 $\mu g\,ml^{-1}$), the viability of cells was evaluated by the MTT method within 24, 48, and 72 h of the post-treatment.

***In vivo* study.** In this study, inbred female BALB/c mice with 6–8 weeks old (purchased from Iran Pasteur Institute) were employed. All mice were conducted within the international guidelines of the Weatherall report and also the national guidelines of the Institutional Animal Care and Use Committee (IACUC) of Tehran University of Medical Sciences.

***In vivo* toxicity of FA@Fe_3O_4 NPs.** To estimate the chronic toxicity dose of the FA@Fe_3O_4 NPs, twenty-five mice were randomly divided into five groups, with five mice in each group. The first group did not receive any injection dose of the nanoparticles and served as the control group. The second to fifth groups were intraperitoneally administrated by using FA@Fe_3O_4 NPs at the doses of 10, 25, 50, and 100 mg kg^{-1}, respectively, for seven consecutive days. The doses were selected based on the initial acute toxicity, which showed FA@Fe_3O_4 NPs are safe at 100 mg kg^{-1} without any adverse effects (data not shown here). likewise, animals acutely treated with the FA@Fe_3O_4 NPs with doses higher than 100 mg kg^{-1} (200 and 500 mg kg^{-1}) showed a significant change in the rate of ALT, ALP and AST compared to the control group ($P < 0.05$). One week after the last injection dose, animals were sacrificed under general anesthesia, and blood samples were taken to evaluate the hematology and clinical chemistry parameters. Red blood cells (RBC), total leukocyte count (WBC), platelets (Plt), mean platelet volume (MPV), hemoglobin (Hgb), hematocrit (Hct), mean corpuscular hemoglobin (MCH), mean cell volume (MCV), mean corpuscular hemoglobin concentration (MCHC), and lymphocytes were measured using an animal blood counter (Celltac; Nihon Kohden, Tokyo, Japan). Plasma urea nitrogen (URE), calcium (Ca), magnesium (Mg), and glucose (Glu) were determined using the CCX System (CCX WB; Nova Biomedical, USA). Plasma alkaline phosphatase (ALP), alanine transaminase (ALT), aspartate transaminase (AST), direct bilirubin (D.Bil), and total protein (TP) were also measured (Autoanalyser Model Biotecnica, BT 3500, Rome, Italy)[57].

Tumor transplantation. The mammary tumor stock (MC4-L2 cells) was aseptically separated from a breast tumor-bearing mouse, and cut into 5 mm fragments and was subcutaneously implanted in the right flank of mice to develop a breast tumor model in the BALB/c mice. After about two weeks, the mammary tumors had grown to about 150–200 mm3 and used for experimentation[58]. In all experiments, animals were anesthetized by subcutaneous injection of a 0.02 ml solution of 100 mg kg^{-1} ketamine and 10 mg kg^{-1} xylazine.

MRI experiments. To evaluate the efficiency of the FA@Fe_3O_4 NPs for the detection and accumulation in the breast cancer tumor tissue, four breast tumor-bearing mice, labeled as 0, 1, 2, and 3, were used in the study. Mouse 0 (control) did not receive any treatment and served as the tumor signal intensity base. Mouse 1 received one dose of the intraperitoneal (IP) injection of the FA@Fe_3O_4 NPs (50 mg kg^{-1}, 50 mg FA@Fe_3O_4 NPs per body

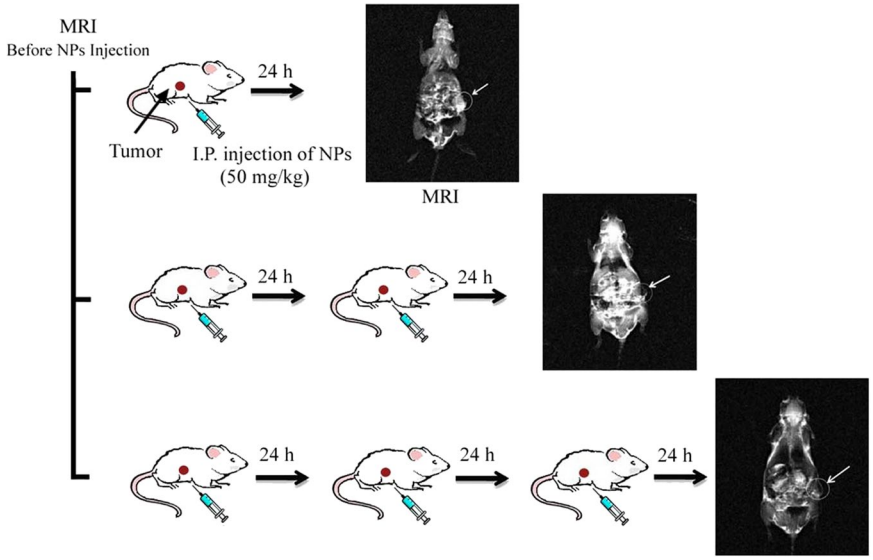

Figure 8. *In vivo* MRI experiments.

weight of mouse), followed by the MRI scanning 24 h after injection. Mouse 2 received two doses of the IP injection of the FA@Fe_3O_4 NPs (50 mg kg^{-1}) with 24 h intervals, followed by the MRI scanning after 48 h of the first injection. Mouse 3 received three doses of the IP injection of the FA@Fe_3O_4 NPs (50 mg kg^{-1}) with 24 h intervals, followed by the MRI scanning after 72 h of the first injection. The MRI experiments were performed using a 3 T MRI scanner (Siemens, MAGNETOM Prisma). All tests were measured by a T_2-weighted spin-echo sequence, and the parameters were set as follows: 3.5 mm slice thickness, TR = 1500, TE = 14.2, 28.4, 42.6, 56.8, 71.0, 85.2, and 99.4 ms, FOV = 180 × 180 mm, and 384 × 384 matrices. Furthermore, the MRI quantification measurements were obtained by evaluating the signal intensity of the tumor region on the T_2-weighted MR images. The MRI experiments are schematically shown in Fig. 8.

ICP-MS analysis of FA@Fe3O4 NPs. Six mice with breast tumors were randomly divided into two groups (three mice in each group) to evaluate the accumulation of the FA@Fe_3O_4 NPs in the breast tumor tissues. The groups were designated as (i) control and (ii) nanoparticles group. Mice in the control group did not receive any treatment and served as the base concentration of Fe in the tumor tissue. Mice in the nanoparticles group received three doses of the IP injection of the FA@Fe_3O_4 NPs (50 mg kg^{-1}) with 24 h interval. Mice were then euthanized 24 h after the last injection, and their tumors were harvested. The concentration of Fe in the tumor tissues was directly analyzed by using inductively coupled plasma mass spectrometry (ICP-MS)[59].

Magnetic Hyperthermia experiments. The heating efficiency of the FA@Fe_3O_4 NPs was evaluated under safe alternating magnetic fields at a constant frequency of 150 kHz and different amplitudes (12.5 and 15.0 mT). To this end, one ml of magnetic suspension (4 $mg_{Fe304}mL^{-1}$) was inserted into an insulated microtube and then placed at the center of the induction coil. It should be noted that the organic content of FA@Fe_3O_4 NPs, measured by thermogravimetric analysis (TGA), was about 37%wt. After applying a certain magnetic field, the temperature rise of the magnetic suspension was recorded versus time. The specific absorption rate (SAR) of the sample was calculated according to the following equation[20]:

$$SAR(Wg^{-1}) = \left(C_{suspension}/X_{NP}\right)(dT/dt) \quad (2)$$

where, $C_{suspension}$ and X_{NP} are the specific heat capacity of the magnetic suspension and the weight fraction of the nanoparticles in the sample, respectively. Also, dT/dt represents the initial slope of the temperature vs time curve. The intrinsic loss power (ILP) value of the samples was determined using the following equation to evaluate the intrinsic heat induction capability of the magnetic fluids and independent of magnetic field intensity and frequency[60]:

$$ILP(nHm^2kg^{-1}) = SAR/f \times H^2 \quad (3)$$

where, f and H are the frequency and intensity of the applied magnetic field, respectively.

To perform MHT using the FA@Fe_3O_4 NPs, twenty-four mice with breast tumors were randomly divided into four groups (6 mice in each group) to investigate the efficacy of MHT. The groups were designated as (i) control, (ii) nanoparticles (NPs), (iii) magnetic field (MF), and (iv) magnetic hyperthermia therapy (MHT). The treatment protocol of each group, including the number of times that FA@Fe_3O_4 NPs were injected and the number of times that the magnetic field was applied is shown in Table 4.

As can be observed in Table 4, the mice in the "control group" were not received any injection of the nanoparticles or exposed to an alternating magnetic field. The mice in the NPs group received six IP injections of the

		Treatment days									
		1	2	3	4	5	6	7	8	9	10
Treatment groups	Control										
	NPs	▼	▼	▼		▼		▼		▼	
	MF				□		□		□		□
	MHT	▼	▼	▼	□	▼	□	▼	□	▼	□

Table 4. Treatment protocol of each group. ▼FA@Fe_3O_4 NPs injection. □Magnetic field.

FA@Fe_3O_4 NPs (50 mg kg^{-1}) on days 1, 2, 3, 5, 7, and 9. The animals in the MF group were exposed four times to a safe alternating magnetic field ($f = 150$ kHz, H = 12.5 mT) for 20 min on days 4, 6, 8, and 10 without any nanoparticle injection. In the fourth group (MHT group), The animals received six injections of the FA@Dex-IO NPs (50 mg kg^{-1}) on days 1, 2, 3, 5, 7, and 9 and also four times exposing to a magnetic field ($f = 150$ kHz, H = 12.5 mT, 20 min) on days 4, 6, 8, and 10. The mice were anesthetized by IP injection of a 0.02 ml solution of 100 mg kg^{-1} ketamine and 10 mg kg^{-1} Xylazine. The tumor volume was measured every other day by using the following equation: tumor volume (mm^3)=tumor length (mm) × tumor width (mm) × tumor width (mm) × $\pi/6$[4,57].

Statistical analysis. Data were analyzed by one-way analysis of variance (ANOVA) and two-tailed Student's t-test using the GraphPad Prism software version 6.0. P values lower than 0.05 were considered to be statistically significant.

Ethical approval. All experiments and procedures were performed according to the guidelines of the Declaration of Helsinki (DOH), and its later amendments or comparable ethical standards. The experimental procedures and the animal use and care protocols were approved by a review board committee of Tehran University of Medical Sciences (TUMS).

Received: 4 July 2019; Accepted: 16 January 2020;
Published online: 03 February 2020

References

1. Soleymani, M., Edrissi, M. & Alizadeh, A. M. Thermosensitive polymer-coated La 0.73 Sr 0.27 MnO 3 nanoparticles: potential applications in cancer hyperthermia therapy and magnetically activated drug delivery systems. *Polymer Journal* **47**, 797 (2015).
2. Soleymani, M., Edrissi, M. & Alizadeh, A. M. Tailoring La 1− x Sr x MnO 3 (0.25≤ x≤ 0.35) nanoparticles for self-regulating magnetic hyperthermia therapy: an *in vivo* study. *Journal of Materials Chemistry B* **5**, 4705–4712 (2017).
3. Shiao, Y.-S., Chiu, H.-H., Wu, P.-H. & Huang, Y.-F. Aptamer-functionalized gold nanoparticles as photoresponsive nanoplatform for co-drug delivery. *ACS applied materials & interfaces* **6**, 21832–21841 (2014).
4. Cazares-Cortes, E. *et al*. Doxorubicin intracellular remote release from biocompatible oligo (ethylene glycol) methyl ether methacrylate-based magnetic Nanogels triggered by magnetic hyperthermia. *ACS applied materials & interfaces* **9**, 25775–25788 (2017).
5. Menon, J. U. *et al*. Dual-drug containing core-shell nanoparticles for lung cancer therapy. *Scientific reports* **7**, 13249 (2017).
6. Guo, H., Sun, H., Zhu, H., Guo, H. & Sun, H. Synthesis of Gd-functionalized Fe 3 O 4@ polydopamine nanocomposites for T 1/T 2 dual-modal magnetic resonance imaging-guided photothermal therapy. *New Journal of Chemistry* **42**, 7119–7124 (2018).
7. Zhou, X. *et al*. Porous MnFe 2 O 4-decorated PB nanocomposites: a new theranostic agent for boosted T 1/T 2 MRI-guided synergistic photothermal/magnetic hyperthermia. *RSC Advances* **8**, 18647–18655 (2018).
8. Arora, S. *et al*. Synthesis, characterization, and evaluation of poly (D, L-lactide-co-glycolide)-based nanoformulation of miRNA-150: potential implications for pancreatic cancer therapy. *International journal of nanomedicine* **9**, 2933 (2014).
9. Wang, H. H. *et al*. Durable mesenchymal stem cell labelling by using polyhedral superparamagnetic iron oxide nanoparticles. *Chemistry–A European Journal* **15**, 12417–12425 (2009).
10. Kim, K. S. & Park, J.-K. Magnetic force-based multiplexed immunoassay using superparamagnetic nanoparticles in microfluidic channel. *Lab on a Chip* **5**, 657–664 (2005).
11. Moroz, P., Jones, S. K. & Gray, B. N. Tumor response to arterial embolization hyperthermia and direct injection hyperthermia in a rabbit liver tumor model. *Journal of surgical oncology* **80**, 149–156 (2002).
12. Wang, L., Dong, J., Ouyang, W., Wang, X. & Tang, J. Anticancer effect and feasibility study of hyperthermia treatment of pancreatic cancer using magnetic nanoparticles. *Oncology reports* **27**, 719–726 (2012).
13. Zhao, Q. *et al*. Magnetic nanoparticle-based hyperthermia for head & neck cancer in mouse models. *Theranostics* **2**, 113 (2012).
14. Jordan, A. *et al*. The effect of thermotherapy using magnetic nanoparticles on rat malignant glioma. *Journal of neuro-oncology* **78**, 7–14 (2006).
15. Attaluri, A. *et al*. Magnetic nanoparticle hyperthermia enhances radiation therapy: A study in mouse models of human prostate cancer. *International Journal of Hyperthermia* **31**, 359–374 (2015).
16. Mahmoudi, K., Bouras, A., Bozec, D., Ivkov, R. & Hadjipanayis, C. Magnetic hyperthermia therapy for the treatment of glioblastoma: a review of the therapy's history, efficacy and application in humans. *International Journal of Hyperthermia* **34**, 1316–1328 (2018).
17. Hu, R. *et al*. Effect of magnetic fluid hyperthermia on lung cancer nodules in a murine model. *Oncology letters* **2**, 1161–1164 (2011).
18. Ludwig, R., Teran, F. J., Teichgraeber, U. & Hilger, I. Nanoparticle-based hyperthermia distinctly impacts production of ROS, expression of Ki-67, TOP2A, and TPX2, and induction of apoptosis in pancreatic cancer. *International journal of nanomedicine* **12**, 1009 (2017).
19. Li, Z. *et al*. Magnetite nanoparticles with high heating efficiencies for application in the hyperthermia of cancer. *Materials Science and Engineering: C* **30**, 990–996 (2010).
20. Shaterabadi, Z., Nabiyouni, G. & Soleymani, M. High impact of *in situ* dextran coating on biocompatibility, stability and magnetic properties of iron oxide nanoparticles. *Materials Science and Engineering: C* **75**, 947–956 (2017).
21. Shaterabadi, Z., Nabiyouni, G. & Soleymani, M. Optimal size for heating efficiency of superparamagnetic dextran-coated magnetite nanoparticles for application in magnetic fluid hyperthermia. *Physica C: Superconductivity and its Applications* **549**, 84–87 (2018).
22. Giustini, A. J. *et al*. Magnetic nanoparticle hyperthermia in cancer treatment. *Nano Life* **1**, 17–32 (2010).

23. Bakoglidis, K., Simeonidis, K., Sakellari, D., Stefanou, G. & Angelakeris, M. Size-dependent mechanisms in AC magnetic hyperthermia response of iron-oxide nanoparticles. *IEEE Transactions on Magnetics* **48**, 1320–1323 (2012).
24. Mehdaoui, B. *et al*. Optimal size of nanoparticles for magnetic hyperthermia: a combined theoretical and experimental study. *Advanced Functional Materials* **21**, 4573–4581 (2011).
25. Ross, J. F., Chaudhuri, P. K. & Ratnam, M. Differential regulation of folate receptor isoforms in normal and malignant tissues *in vivo* and in established cell lines. *Physiologic and clinical implications. Cancer* **73**, 2432–2443 (1994).
26. Gao, G. *et al*. Shape-controlled synthesis and magnetic properties of monodisperse Fe3O4 nanocubes. *Crystal Growth & Design* **10**, 2888–2894 (2010).
27. Hemery, G. *et al*. Tuning sizes, morphologies, and magnetic properties of monocore versus multicore iron oxide nanoparticles through the controlled addition of water in the polyol synthesis. *Inorganic chemistry* **56**, 8232–8243 (2017).
28. Ahmadi, S., Chia, C.-H., Zakaria, S., Saeedfar, K. & Asim, N. Synthesis of Fe3O4 nanocrystals using hydrothermal approach. *Journal of Magnetism and Magnetic Materials* **324**, 4147–4150 (2012).
29. Goh, S. *et al*. Hydrothermal preparation of high saturation magnetization and coercivity cobalt ferrite nanocrystals without subsequent calcination. *Materials Chemistry and Physics* **120**, 31–35 (2010).
30. Li, Q. *et al*. Correlation between particle size/domain structure and magnetic properties of highly crystalline Fe 3 O 4 nanoparticles. *Scientific reports* **7**, 9894 (2017).
31. Klug, H. P. & Alexander, L. E. X-ray diffraction procedures: for polycrystalline and amorphous materials. X-Ray Diffraction Procedures: For Polycrystalline and Amorphous Materials, 2nd Edition, by Harold P. Klug, Leroy E. Alexander, pp. 992. ISBN 0-471-49369-4. Wiley-VCH, May 1974, 992 (1974).
32. Dat, T. Q. Study On Influence Of Temperature And Duration Of Hydrothermal Treatment To Properties Of Nano Ferrite $NiFe_2O_4$ Materials. *Vietnam Journal of Science and Technology* **54**, 1 (2016).
33. Jalili, H., Aslibeiki, B., Varzaneh, A. G. & Chernenko, V. A. The effect of magneto-crystalline anisotropy on the properties of hard and soft magnetic ferrite nanoparticles. *Beilstein journal of nanotechnology* **10**, 1348–1359 (2019).
34. Habib, A., Ondeck, C., Chaudhary, P., Bockstaller, M. & McHenry, M. Evaluation of iron-cobalt/ferrite core-shell nanoparticles for cancer thermotherapy. *Journal of Applied Physics* **103**, 07A307 (2008).
35. Alonso, J. *et al*. FeCo nanowires with enhanced heating powers and controllable dimensions for magnetic hyperthermia. *Journal of Applied Physics* **117**, 17D113 (2015).
36. Mehdaoui, B. *et al*. Large specific absorption rates in the magnetic hyperthermia properties of metallic iron nanocubes. *Journal of Magnetism and Magnetic Materials* **322**, L49–L52 (2010).
37. Sathya, A. *et al*. Co x Fe3–x O4 nanocubes for theranostic applications: effect of cobalt content and particle size. *Chemistry of Materials* **28**, 1769–1780 (2016).
38. Tan, R., Carrey, J. & Respaud, M. Magnetic hyperthermia properties of nanoparticles inside lysosomes using kinetic Monte Carlo simulations: Influence of key parameters and dipolar interactions, and evidence for strong spatial variation of heating power. *Physical Review B* **90**, 214421 (2014).
39. Nemati, Z. *et al*. Improving the heating efficiency of iron oxide nanoparticles by tuning their shape and size. *The Journal of Physical Chemistry C* **122**, 2367–2381 (2018).
40. Zhang, J., Rana, S., Srivastava, R. & Misra, R. On the chemical synthesis and drug delivery response of folate receptor-activated, polyethylene glycol-functionalized magnetite nanoparticles. *Acta Biomaterialia* **4**, 40–48 (2008).
41. Arun, T., Prabakaran, K., Udayabhaskar, R., Mangalaraja, R. & Akbari-Fakhrabadi, A. Carbon decorated octahedral shaped Fe3O4 and α-Fe2O3 magnetic hybrid nanomaterials for next generation supercapacitor applications. *Applied Surface Science* **485**, 147–157 (2019).
42. Azcona, P., López-Corral, I. & Lassalle, V. Fabrication of folic acid magnetic nanotheranostics: An insight on the formation mechanism, physicochemical properties and stability in simulated physiological media. *Colloids and Surfaces A: Physicochemical and Engineering Aspects* **537**, 185–196 (2018).
43. Wang, Z. *et al*. Folic acid modified superparamagnetic iron oxide nanocomposites for targeted hepatic carcinoma MR imaging. *RSC Advances* **4**, 7483–7490 (2014).
44. Hao, H., Ma, Q., Huang, C., He, F. & Yao, P. Preparation, characterization, and *in vivo* evaluation of doxorubicin loaded BSA nanoparticles with folic acid modified dextran surface. *International journal of pharmaceutics* **444**, 77–84 (2013).
45. Hoshyar, N., Gray, S., Han, H. & Bao, G. The effect of nanoparticle size on *in vivo* pharmacokinetics and cellular interaction. *Nanomedicine* **11**, 673–692 (2016).
46. Thanh, N. T. Magnetic nanoparticles: from fabrication to clinical applications. (CRC press, 2012).
47. Biswas, S., Kumari, P., Lakhani, P. M. & Ghosh, B. Recent advances in polymeric micelles for anti-cancer drug delivery. *European Journal of Pharmaceutical Sciences* **83**, 184–202 (2016).
48. Hergt, R. *et al*. Physical limits of hyperthermia using magnetite fine particles. *IEEE Transactions on magnetics* **34**, 3745–3754 (1998).
49. Atkinson, W. J., Brezovich, I. A. & Chakraborty, D. P. Usable frequencies in hyperthermia with thermal seeds. *IEEE Transactions on Biomedical Engineering*, 70–75 (1984).
50. Glöckl, G. *et al*. The effect of field parameters, nanoparticle properties and immobilization on the specific heating power in magnetic particle hyperthermia. *Journal of Physics: Condensed Matter* **18**, S2935 (2006).
51. Shah, R. R., Davis, T. P., Glover, A. L., Nikles, D. E. & Brazel, C. S. Impact of magnetic field parameters and iron oxide nanoparticle properties on heat generation for use in magnetic hyperthermia. *Journal of magnetism and magnetic materials* **387**, 96–106 (2015).
52. Bellizzi, G., Bucci, O. M. & Chirico, G. Numerical assessment of a criterion for the optimal choice of the operative conditions in magnetic nanoparticle hyperthermia on a realistic model of the human head. *International Journal of Hyperthermia* **32**, 688–703 (2016).
53. Samanta, B. *et al*. Protein-passivated Fe_3O_4 nanoparticles: low toxicity and rapid heating for thermal therapy. *Journal of materials chemistry* **18**, 1204–1208 (2008).
54. Hergt, R. & Dutz, S. Magnetic particle hyperthermia—biophysical limitations of a visionary tumour therapy. *Journal of Magnetism and Magnetic Materials* **311**, 187–192 (2007).
55. Huang, H. S. & Hainfeld, J. F. Intravenous magnetic nanoparticle cancer hyperthermia. *International journal of nanomedicine* **8**, 2521 (2013).
56. Zhou, Q. *et al*. Target-specific cellular uptake of folate-decorated biodegradable polymer micelles. *The Journal of Physical Chemistry B* **115**, 12662–12670 (2011).
57. Mohsenikia, M. *et al*. The protective and therapeutic effects of alpha-solanine on mice breast cancer. *European journal of pharmacology* **718**, 1–9 (2013).
58. Isanejad, A. *et al*. MicroRNA-206, let-7a and microRNA-21 pathways involved in the anti-angiogenesis effects of the interval exercise training and hormone therapy in breast cancer. *Life sciences* **151**, 30–40 (2016).
59. Salimi, M. *et al*. Biodistribution, pharmacokinetics, and toxicity of dendrimer-coated iron oxide nanoparticles in BALB/c mice. *International journal of nanomedicine* **13**, 1483 (2018).
60. Shaterabadi, Z., Nabiyouni, G. & Soleymani, M. Physics responsible for heating efficiency and self-controlled temperature rise of magnetic nanoparticles in magnetic hyperthermia therapy. *Progress in biophysics and molecular biology* **133**, 9–19 (2018).
61. Pradhan, P. *et al*. Comparative evaluation of heating ability and biocompatibility of different ferrite-based magnetic fluids for hyperthermia application. *Journal of Biomedical Materials Research Part B: Applied Biomaterials: An Official Journal of The Society*

for Biomaterials, The Japanese Society for Biomaterials, and The Australian Society for Biomaterials and the Korean Society for Biomaterials **81**, 12–22 (2007).
62. Nomura, S. *et al*. Inductive heating of mg ferrite powder in high-water content phantoms using AC magnetic field for local hyperthermia. *Heat Transfer Engineering* **28**, 1017–1022 (2007).
63. Salunkhe, A. B., Khot, V. M., Ruso, J. M. & Patil, S. Water dispersible superparamagnetic Cobalt iron oxide nanoparticles for magnetic fluid hyperthermia. *Journal of Magnetism and Magnetic Materials* **419**, 533–542 (2016).
64. Jasso-Terán, R. A. *et al*. Synthesis, characterization and hemolysis studies of Zn (1− x) CaxFe2O4 ferrites synthesized by sol-gel for hyperthermia treatment applications. *Journal of Magnetism and Magnetic Materials* **427**, 241–244 (2017).
65. Thorat, N. D., Bohara, R. A., Yadav, H. M. & Tofail, S. A. Multi-modal MR imaging and magnetic hyperthermia study of Gd doped Fe_3O_4 nanoparticles for integrative cancer therapy. *RSC Advances* **6**, 94967–94975 (2016).
66. Brollo, M. *et al*. Magnetic hyperthermia in brick-like Ag@ Fe_3O_4 core–shell nanoparticles. *Journal of Magnetism and Magnetic Materials* **397**, 20–27 (2016).
67. Brusentsov, N. A. *et al*. Evaluation of ferromagnetic fluids and suspensions for the site-specific radiofrequency-induced hyperthermia of MX11 sarcoma cells *in vitro*. *Journal of Magnetism and Magnetic Materials* **225**, 113–117 (2001).
68. Jordan, A., Rheinländer, T., Waldöfner, N. & Scholz, R. Increase of the specific absorption rate (SAR) by magnetic fractionation of magnetic fluids. *Journal of Nanoparticle Research* **5**, 597–600 (2003).
69. Lee, J.-H. *et al*. Exchange-coupled magnetic nanoparticles for efficient heat induction. *Nature nanotechnology* **6**, 418 (2011).
70. Jang, Jt *et al*. Giant Magnetic Heat Induction of Magnesium-Doped γ-Fe_2O_3 Superparamagnetic Nanoparticles for Completely Killing Tumors. *Advanced Materials* **30**, 1704362 (2018).

Acknowledgements

This study was funded by Tehran University of Medical Sciences (Grant number: 28356 and 27707). We also are grateful for the financial support received from the Iran National Science Foundation (INSF) (Grant number: 94016256). None of the funding sources had any role in the study design, the collection, the analysis and interpretation of data, the writing of the report, or the decision to submit the article for publication.

Author contributions

M. Soleymani and A.M. Alizadeh: study conception and design, data analysis, and manuscript preparation. Z. Shaterabadi, S. Khalighfard, S. Khodayari, H.Khodayari, and: M.R. Kalhori: sample collection, sample processing, and data analysis. M. Hadjighassem: study conception.

Competing interests

The authors declare no competing interests.

Additional information

Correspondence and requests for materials should be addressed to A.M.A.

Reprints and permissions information is available at www.nature.com/reprints.

Publisher's note Springer Nature remains neutral with regard to jurisdictional claims in published maps and institutional affiliations.